RSC Advances

PAPER

View Article Online
View Journal | View Issue

Cite this: *RSC Adv.*, 2022, **12**, 3838

Fabrication of durable underoil superhydrophobic surfaces with self-cleaning and oil–water separation properties†

Wanfei Ren, Zhongxu Lian,* Jiaqi Wang, Jinkai Xu* and Huadong Yu

In this study, a simple method without any additional chemical modification is proposed to fabricate underoil superhydrophobic surfaces with micro- and nano-hierarchical structures using a nanosecond laser system. The fabricated surfaces exhibited extreme superhydrophobicity and underoil superhydrophobicity with high contact angles of 153.8 ± 1.5° and 161.3 ± 1.1°, respectively. The results show that even after 20 abrasion cycles, the fabricated surfaces retained water repellency and self-cleaning performance under oil, while the superhydrophobicity in air was not resistant to wear. In addition, the fabricated brass meshes can also be used to separate oil in an oil–water mixture based on the prewetting induced underoil superhydrophobicity after being damaged. The separation efficiency was as high as 97.8%, which made them more appropriate for the oil–water separation than those based on superhydrophobicity. The proposed fabrication method is suitable for large-scale and mass production and provides a new avenue and possibility for further development of robust functional interface materials.

Received 25th August 2021
Accepted 25th January 2022

DOI: 10.1039/d1ra06422c

rsc.li/rsc-advances

1. Introduction

Superhydrophobic surfaces with a water contact angle larger than 150° and a sliding angle smaller than 10° can be found in many animals and plants in nature.[1,2] Recently, they have attracted much attention owing to their potential application in the fields of self-cleaning, anti-icing, corrosion resistance, oil/water separation and microfluidics.[3–8] Despite the success of the fabrication of superhydrophobic surfaces without any additional chemical modification,[9–11] mechanical wear is usually revealed as increased sticking of water, especially for the hydrophilic metal materials, resulting in loss of the non-wetting properties owing to the exposure of hydrophilic materials.[12,13] In response to this challenge, materials with superhydrophobic properties under oil, which are characterized by high water contact angle and low sliding angle under oil, have been introduced. They have potential applications in many fields, including self-cleaning, anti-fouling and oil/water separation.[14,15] Underoil superhydrophobic materials have the advantage of the oil-favoring properties that allow oil absorption near the material's surface, which minimizes the contact between the solid surface and water in an oil/water/solid three-phase system, so that the substrate shows extreme water-repellent behavior when submerged into the oil. Thus far, there have been fewer studies on the preparation and application of underoil superhydrophobic materials. Tian *et al.*[16] prepared an underwater superoleophobic and underoil superhydrophobic surface using the combination of re-entrant surface curvatures and delicately matched surface chemistry. They have pointed out that metastable states are necessary to achieve unusual wetting phenomenon. Lu *et al.*[17] used the coating method to create a robust self-cleaning surface that could function when exposed to oil. Although the self-cleaning and oil–water separation performances of underoil superhydrophobic materials have been verified,[18–20] their advantage of the underoil superhydrophobic property compared with the superhydrophobic property in the air, has not been profoundly studied, and there has not been sufficient basis for selection of underoil superhydrophobic materials. Moreover, the current fabrication methods of underoil superhydrophobic materials are complex and costly. Thus, it is necessary to develop a simple fabrication method of underoil superhydrophobic materials.

To address this challenge, this work proposes a simple fabrication method of underoil superhydrophobic brass surfaces with self-cleaning properties in the air and oil based on laser-ablated technology. The proposed method does not require any chemical modification and is suitable for large-scale and mass production. The durability of surfaces has been evaluated using the mechanical abrasion test, and the results show that the fabricated surfaces can remain excellent underoil water-repellent and self-cleaning properties and high separation efficiency even after abrasion. The proposed method opens

Ministry of Education Key Laboratory for Cross-Scale Micro and Nano Manufacturing, Changchun University of Science and Technology, Changchun, 130022, China. E-mail: lianzhongxu@cust.edu.cn; xujinkai2000@163.com.cn

† Electronic supplementary information (ESI) available. See DOI: 10.1039/d1ra06422c

a new avenue for the development of durable functional materials with self-cleaning and oil–water separation properties.

2. Materials and methods

2.1 Materials

Brass plates (H62) were purchased from Northwest Institute of Nonferrous Metal Company, which were composed of 61.1% Cu and 38.9% Zn. The brass meshes (H62) were purchased from Hebei Lijie Metal Wire Mesh Manufacturing Co. Ltd, which were composed of 63.1% Cu and 36.9% Zn. The kerosene was purchased from China Petroleum & Chemical Co., Ltd. The soybean oil was purchased from Kerry Oil Co., Ltd. The dodecane, hexadecane, and chloroform were purchased from Sigma-Aldrich. Absolute ethanol, acetone, and silicone oil were purchased from Jilin Hao Di Chemical Reagent Co., Ltd. The distilled water with a resistivity larger than 1 MΩ cm was used in all of the experiments.

2.2 Sample fabrication

The micro- and nano-scale hierarchical morphologies of the brass surfaces were formed by a Q-switched nanosecond laser marking system (Han's Laser YLP-ST20E) with a wavelength of 1064 nm and a pulse width of 100 ns through the line-by-line scanning process. The Q frequency, scanning speed and interval were set to 20 kHz, 500 mm s^{-1} and 10 μm, respectively, as shown in Fig. 1a and b. The basic concept of laser technique used for the brass mesh fabrication is schematically presented in Fig. S1,†[21] where it can be seen that the laser penetrated the transparent confining layer and focused on the brass mesh. The silica glass with the size of 100 mm × 100 mm × 2 mm was selected as a confining layer to ensure the laser focus point would be at the brass mesh surfaces. After the laser-ablated treatment, the brass plates (meshes) were left in the air for 30 days to obtain superhydrophobicity and underoil superhydrophobicity, as shown in Fig. 1c and d.[22]

2.3 Stability measurement

In the sandpaper abrasion test, a weight of 100 g was used on the brass (mesh) surfaces to examine their mechanical stability. During the test, the surfaces were placed on the sandpaper (800 mesh) and moved for 10 cm along the ruler. Then, the surfaces were rotated by 90° and moved for another 10 cm. The process is defined as two abrasion cycles. Before recording the underoil water contact angle, the debris on the abraded samples was removed with a soft cloth when submerged in the water. The micro- and nano-scale morphologies were characterized by a scanning electron microscope (SEM) both before and after the sandpaper abrasion test.

2.4 Oil/water separation

As a proof-of-concept of the oil/water separation of underoil superhydrophobic surfaces based on the gravity-driven mechanism, an as-fabricated mesh prewetted by the oil was used. Next, a mixture of oil (20 g) and water (20 g) was poured onto the prewetted mesh. A high-precision electronic balance (AUW120D) was used to measure the weight before and after liquid separation, and then the separation efficiency of samples was calculated. The micro- and nano-scale morphologies before and after 20 abrasion cycles with the sandpaper were characterized by SEM.

2.5 Characterization

A scanning electron microscope (ZEISS EVO 20) was used to analyze the micro- and nano-scale hierarchical morphologies at an accelerating voltage of 20 kV. The optical images were obtained using a digital camera (EOS M3). The chemical composition was characterized by an X-ray diffractometer (XRD, D/Max-2500) and an energy dispersive X-ray spectroscopy (EDS, X-Max). The water contact angles and sliding angles were measured at 20 °C by a contact angle measuring instrument (Kruss DSA100) using water droplets of 5 μL and 20 μL, and for each sample, an average value of every three successive

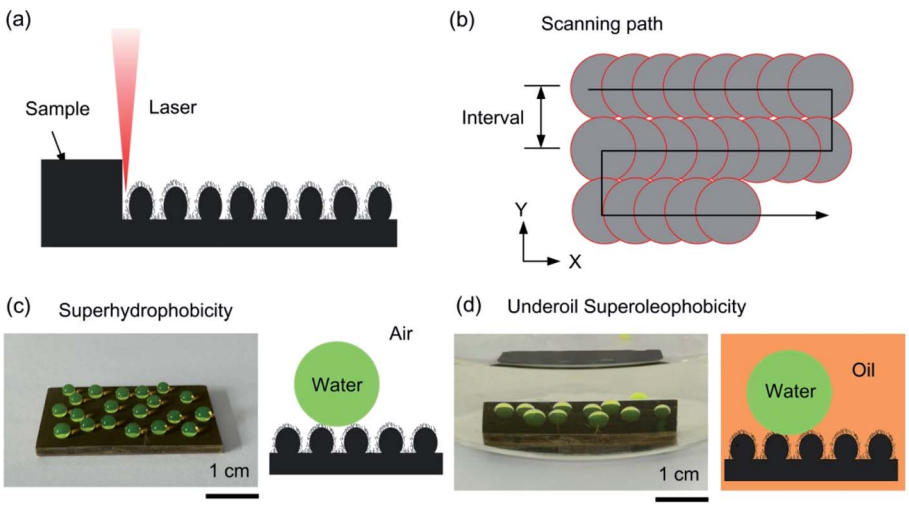

Fig. 1 (a and b) Schematic diagram of laser processing and scanning path. (c) Water droplets on the fabricated surface in the air. (d) Water droplets on the fabricated surface under oil.

measurements was calculated. To measure the wettability of water droplets under different types of oils, kerosene, soybean oil, dodecane, hexadecane, and chloroform were used. In the following discussion, kerosene was used in the experiments unless specified otherwise. For the wettability under oil, a transparent container bonded by an acrylic plate was used to hold the medium oil. The schematic diagram of the wettability measurement is shown in Fig. S2.†

3. Results and discussion

3.1 Surface topography and chemical composition

The surface morphology of oxide coatings obtained at different powers and intervals of the scan line was characterized by the SEM. The SEM and cross-sectional images of the as-fabricated surfaces at 6 W, 12 W, and 18 W are presented in Fig. 2. After the laser-ablated process, the three as-fabricated surfaces were rough. The SEM images in Fig. 2(a1–c1) show that the micro-flower-like structures with the size of 10 μm were irregularly distributed on the surface, and the higher power led to the formation of larger microstructures on the surface. The high magnification SEM images show that the nano-villus-like structures could be observed on the micro-flower-like structures with the increase in power, as shown in Fig. 2(a2–c2). The nano-villus-like structures were formed due to the melting and re-solidification of the materials in the laser-ablated process. The sample's cross-sectional view shown in Fig. 2(a3–c3) indicates that the surface obtained at high power was more textured than that obtained at low power.

The XRD and EDS were used to characterize the chemical composition of the brass surfaces fabricated by the laser-ablated technology. Fig. 3a shows the XRD patterns of the as-fabricated surfaces obtained at different powers. The characteristic peaks of the surfaces at 31.17°, 42.22°, 43.42°, 49.32°, 63.27°, 72.27°, 79.72° and 95.52°, which were obtained at different powers were in good agreement with the polished brass surface, indicating that there was no new peak for the surfaces fabricated using the nanosecond laser. The reason for this could be that species formed by the laser-ablated process were amorphous and could not be detected by the XRD. Moreover, element O was observed in the EDS analysis results of the as-fabricated surfaces, as shown in Fig. 3b–d, and its content increased with the power. The results indicated that the oxide coating was successfully formed on the brass substrates.

3.2 Wettability analysis

As shown in Fig. 4a and b, under the power of 12 W, the laser-ablated surface had the superhydrophobicity and oleophilicity in the air with a water contact angle of 153.8 ± 1.5° and an oil contact angle of 13.4 ± 0.5°, respectively. Fig. 4c shows the image of underoil water droplets with an approximately spherical shape on the surface and a water contact angle of 161.3 ± 1.1°, indicating an excellent underoil superhydrophobicity. The reason for this could be that the oil wetted the microstructure due to the oleophilicity of the surface when it was placed in an oil environment. The formed oil film on the microstructure prevented the water droplet from directly contacting the surface, thus ensuring the

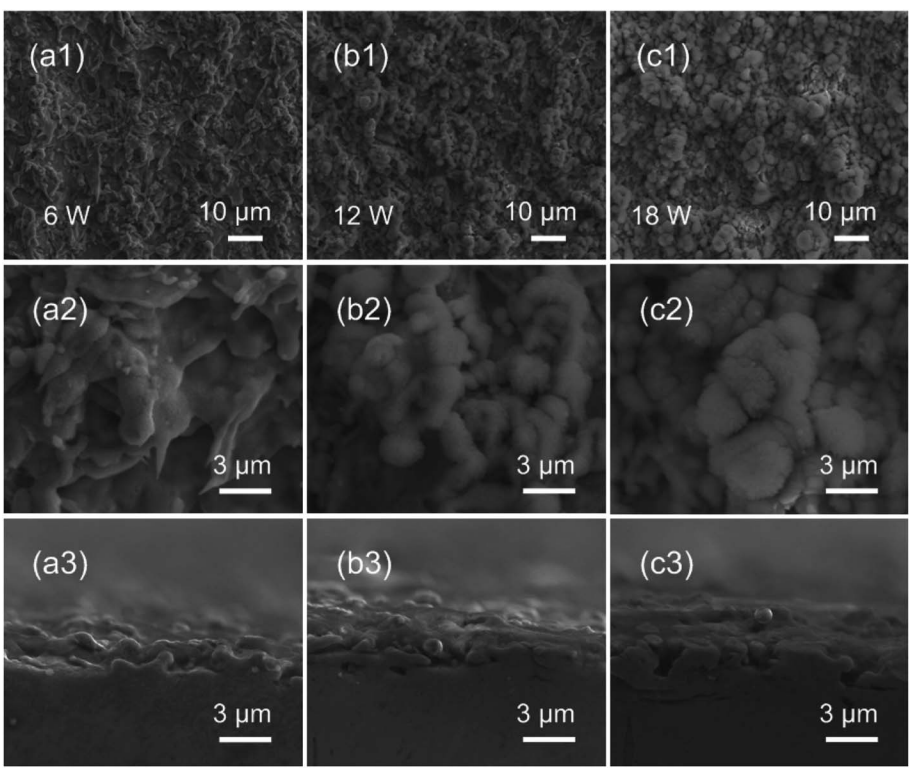

Fig. 2 SEM and cross-sectional images of as-fabricated surfaces at (a) 6 W, (b) 12 W and (c) 18 W.

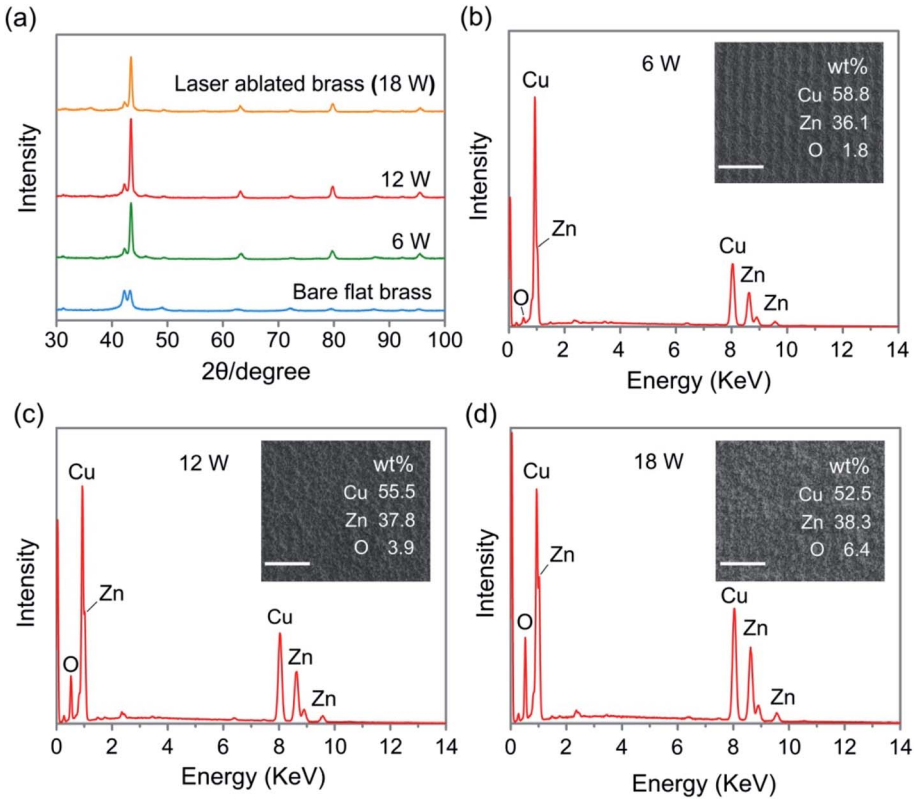

Fig. 3 (a) XRD patterns and (b–d) EDS spectra of the surfaces fabricated with different powers.

surface's superhydrophobicity under oil. Moreover, the surface had an ultra-low water adhesion under oil, as shown in Fig. 4d. Fig. 4e illustrates the rolling process of a water droplet under the gravitation effect, where it can be seen that the water droplet could roll off easily from the 1°-tilted surface under oil. The superhydrophobic property of the surface was tested under the different types of oils, including kerosene, soybean oil, silicone oil, dodecane, hexadecane, and chloroform (Fig. 4f), and all of the water contact angles of the as-fabricated surface were greater than 150°. The wettability of the brass surfaces obtained with different powers was measured under oil, as shown in Fig. 5. For the polished brass surface (the power was zero), the water droplet under the oil exhibited weak hydrophobicity with the contact angle of 138.8 ± 2.7°. As the power increased from 3 W to 18 W, the underoil water contact angle of the surface increased slightly from 159.3 ± 1.1° to 162.4 ± 0.9° while the sliding angle decreased, indicating that under the oil, the surface's wettability varied from the hydrophobicity to superhydrophobicity.

3.3 Mechanical stability analysis of underoil superhydrophobic surface

Surface durability is a very important factor, which indicates the possibility of widespread application of special wettability surfaces.[12,23–28] The micro- and nano-hierarchical structures are mechanically weak and can be easily destroyed by a physical impact and friction, resulting in the removal of a substantial amounts of material.[12] We described interaction of the underoil water-repellent surfaces in the abrasion test, and characterized the structure and wettability of the surfaces fabricated under the power of 12 W. During the test, a weight of 100 g was applied on the surfaces with the size of 2 cm × 3.5 cm. After 20 abrasion cycles, the SEM results revealed that the repeated abrasion with the sandpaper led to scratching, and a large amount of material was removed from on the surface (Fig. 6a). As shown in Fig. 6b, severe physical damage had a slight effect on the underoil water contact angle, and the contact angle decreased from 161.3 ± 1.1° to 159.5 ± 1.9°. Correspondingly, the underoil water sliding angle changed from 0.9 ± 0.3° to 18.1 ± 2.3°. The results showed that the abraded surfaces maintained an excellent water-repellent property when exposed to the oil as presented in Movie S1.† Although the hierarchical structures could be damaged and the hydrophilic bulk materials could be exposed after the exposure of the surface in the abrasion test, the water-repellent behavior of the surface remained stable to a certain extent, which was due to the oil absorption nature of the bulk materials and the change in the micro- and nano-hierarchical morphology that was sufficient to maintain the underoil water-repellent property, as shown in Fig. 6c and d. However, as shown in Fig. 6e, for the wettability of the abraded surfaces in air, the contact angle and the sliding angle changed significantly by decreasing from 153.8 ± 1.5° to 137.1 ± 4.7° and increasing from 2.6 ± 0.7° to 90°, respectively. The water droplet adhered to the abraded surface without sliding in Wenzel model,[29] as shown in Fig. 6f and Movie S2.†

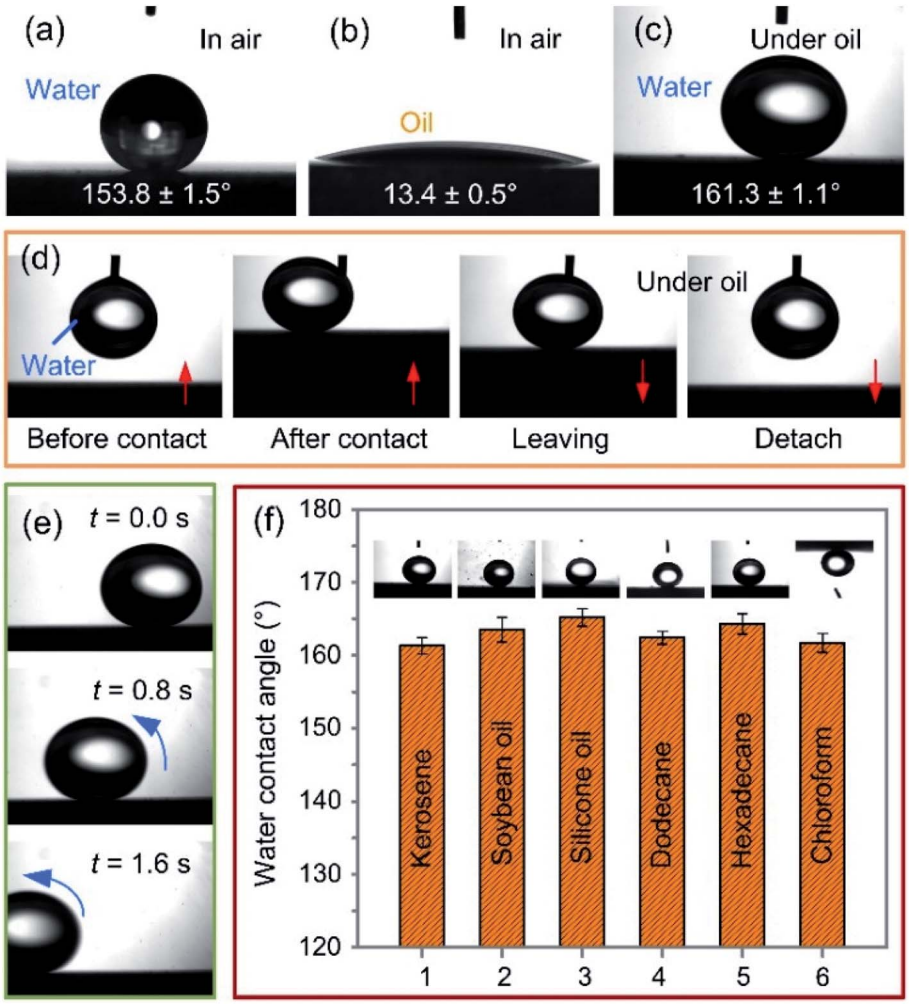

Fig. 4 (a and b) Water and oil contact angles of the laser-ablated surface in the air. (c) Water contact angle of the surface under oil. (d) Low adhesion behavior of the water droplet to the surface under oil. (e) Rolling process of a water droplet on the 1°-tilted surface under oil. (f) Water contact angle of the surface under the different types of oils.

3.4 Self-cleaning property and its mechanical stability analysis

The loss of superwetting properties of interface materials due to the damage of the micro- and nano-hierarchical structures can affect their function and thus can immensely impact their applications. Recently, underoil superhydrophobic surfaces and meshes have been developed for achieving self-cleaning property and oil–water separation. Weak water-repellent property has been one of the main issues as well.

We subsequently studied the self-cleaning property of the surfaces fabricated by the laser-ablated process. The underoil superhydrophobic surfaces showed a good self-cleaning property in both air and oil. As presented in Movies S3 and S4,† water droplets could roll off easily from the slightly sloped surface and take away the Fe powders when exposed to both air and oil. After 20 abrasion cycles, the self-cleaning property of the abraded surfaces was demonstrated. As shown in Fig. 7a, when the abraded surface was under oil, the Fe powders on the surface could be easily removed by water droplets because of the excellent water-repellent property of the surface (Fig. 6c). The results showed that the surfaces maintained an excellent self-cleaning property when being abraded, even after 20 abrasion cycles of their exposure to the oil. However, when the self-cleaning test was performed in air, Fe powders could not be easily removed by water droplets, as shown in Fig. 7b. The droplet with Fe powders, namely, droplets 1, 2, 6 and 9, easily adhered to the surface. Only when another droplet was merged with the adhered droplet, for instance, when droplets 1 and 3, droplets 6 and 7 were merged, the Fe powders could be rejected by a large merged droplet, namely, droplets 4 and 8, respectively. The reason for this phenomenon was that the abraded surface had the adhesion property for droplets, as shown in Fig. 6f. The results show that the underoil superhydrophobic surfaces had a more durable self-cleaning performance.

3.5 Oil/water separation and mechanical stability of underoil superhydrophobic meshes

In addition to the self-cleaning property, the oil–water separation performance of the laser-ablated brass mesh was

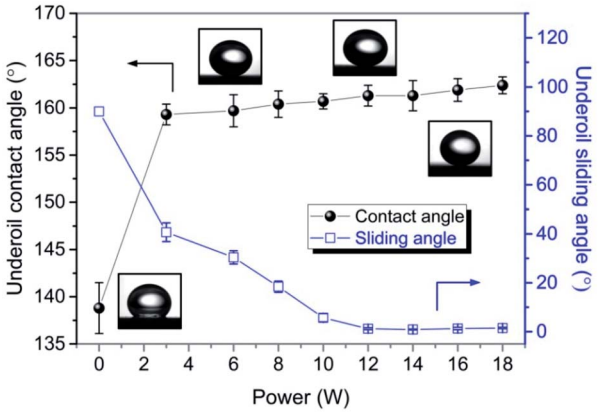

Fig. 5 Underoil water-wettability of the brass surfaces obtained with different powers.

investigated. In the sandpaper abrasion test, a weight of 100 g was applied to the meshes with the size of 5 cm × 5 cm. The SEM images of the mesh fabricated under a power of 12 W before and after 10 abrasion cycles are presented in Fig. 8a–d. For the abraded mesh, a certain amount of material was removed from the wire of the mesh. However, the abraded mesh maintained an excellent water-repellent property when being exposed to the oil. As shown in Fig. 8e, the contact angle of the abraded mesh decreased from 152.4 ± 1.9° to 151.1 ± 2.8°, and the underoil water sliding angle changed from 1.8 ± 1.6° to 4.9 ± 1.5°. For the wettability of the abraded mesh in air, the contact angle and sliding angle changed significantly, decreasing from 151.9 ± 2.1° to 149.1 ± 3.2° and increasing from 3.7 ± 1.9° to 53.7 ± 5.1°, respectively, as shown in Fig. 8f. The results demonstrated that the abraded mesh lost its excellent superhydrophobic property in the air.

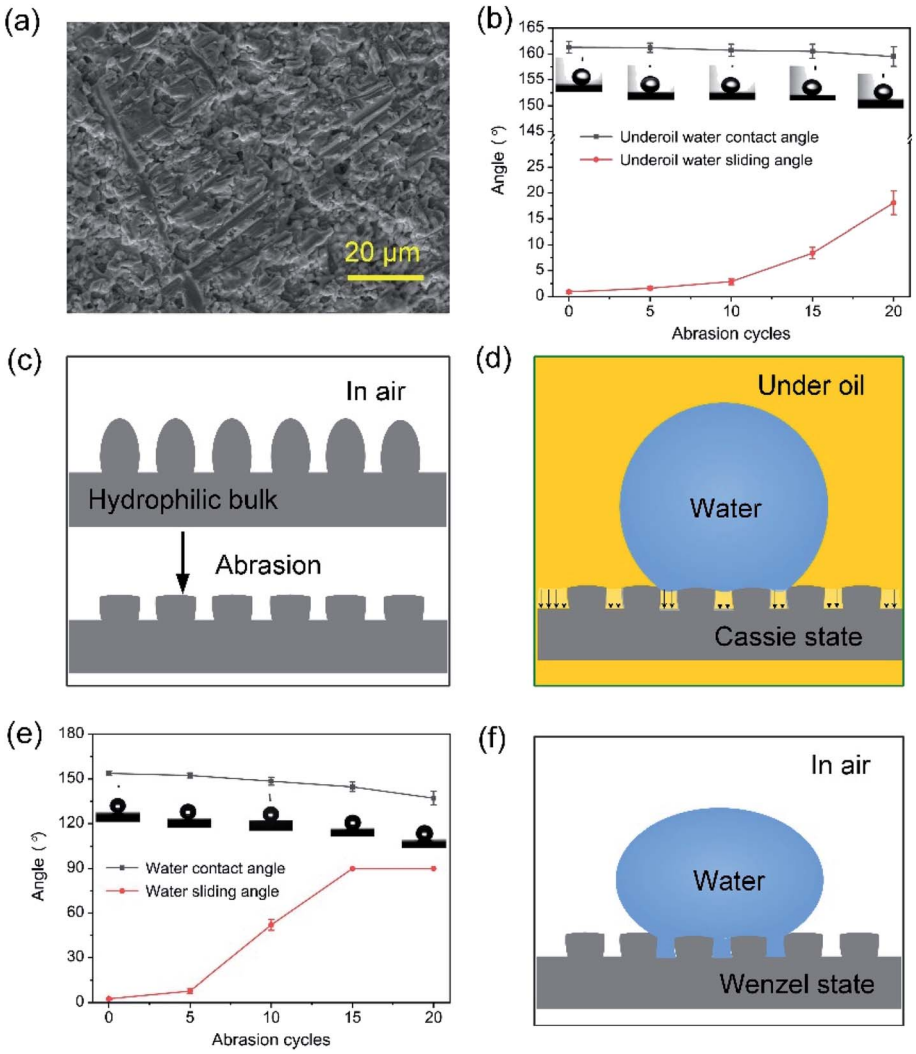

Fig. 6 (a) SEM image of the underoil water-repellent surface after 20 abrasion cycles. (b) Underoil water contact angle and sliding angle of the surface after different abrasion cycles. (c) Exposed hydrophilic bulk materials after the abrasion test. (d) Underoil water-repellent property of the abraded surface in Cassie model. (e) Water contact angle and sliding angle of the surface after different abrasion cycles in air. (f) Water droplet adhered to the abraded surface in Wenzel model.

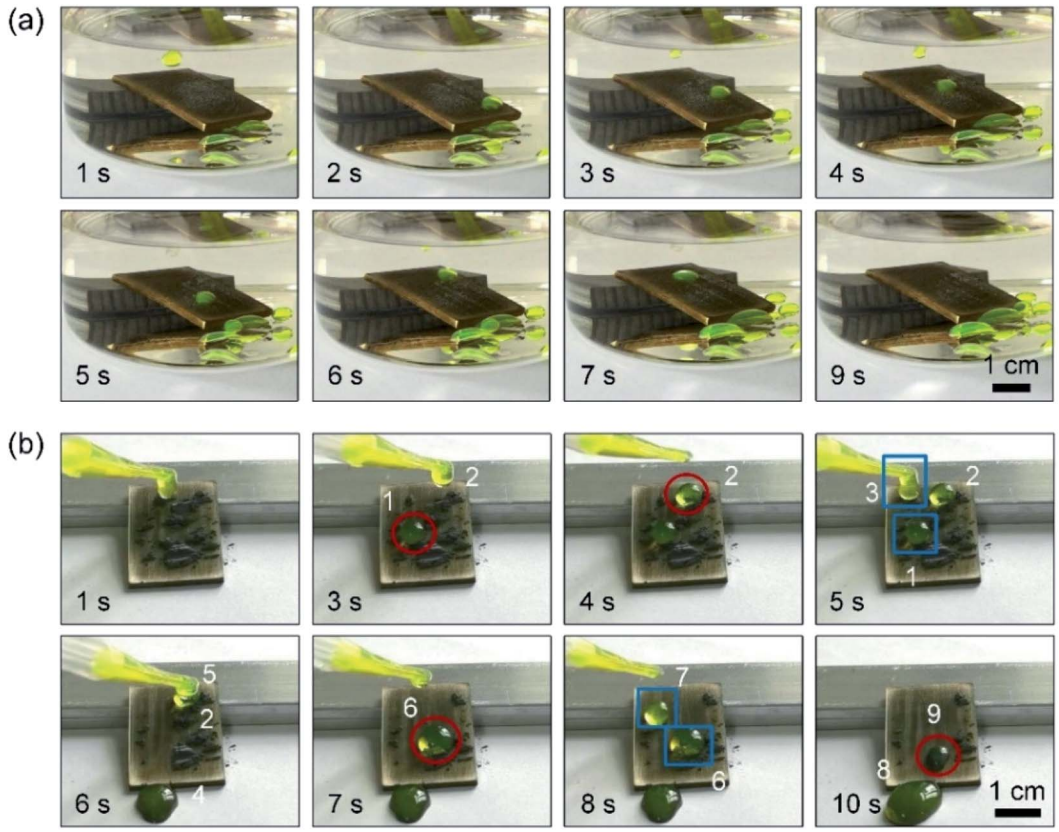

Fig. 7 Self-cleaning performances of the abraded surface in both (a) oil and (b) air.

The oil–water separation was performed using homemade devices, driven solely by gravity without applying any external pressure. Before the sandpaper abrasion test, when the mixture of water and chloroform was poured onto the mesh prewetted with chloroform, the water dyed red was accumulated on the mesh, but the chloroform quickly penetrated through the pre-wetted mesh and felt into the collection container, as shown in Movie S5.† The separation efficiency was 98.1%, which

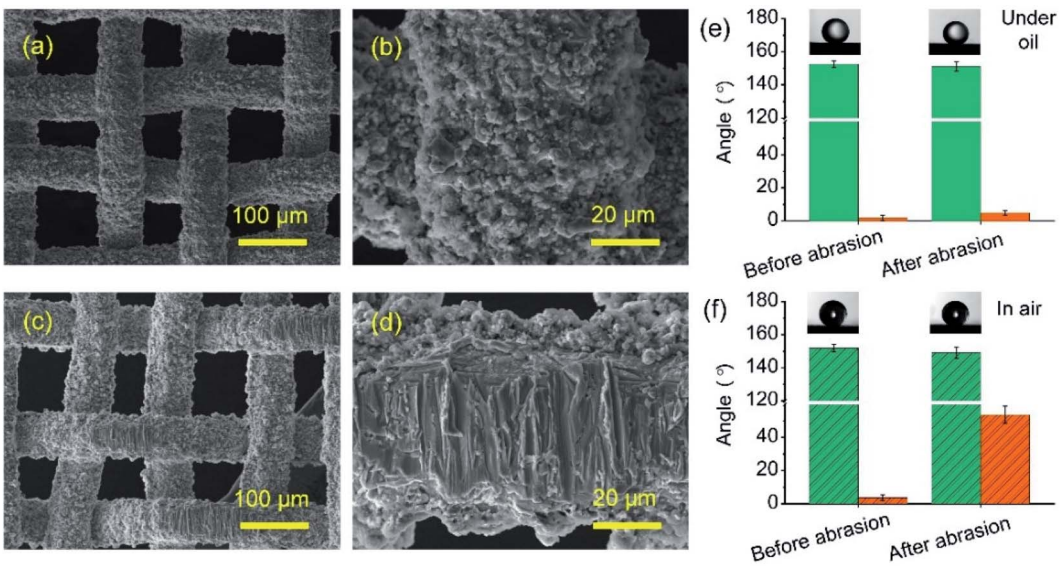

Fig. 8 SEM images of the mesh (a and b) before and (c and d) after 10 abrasion cycles. Contact angle ( ) and sliding angle ( ) of the mesh before and after abrasion (e) under oil and (f) in the air.

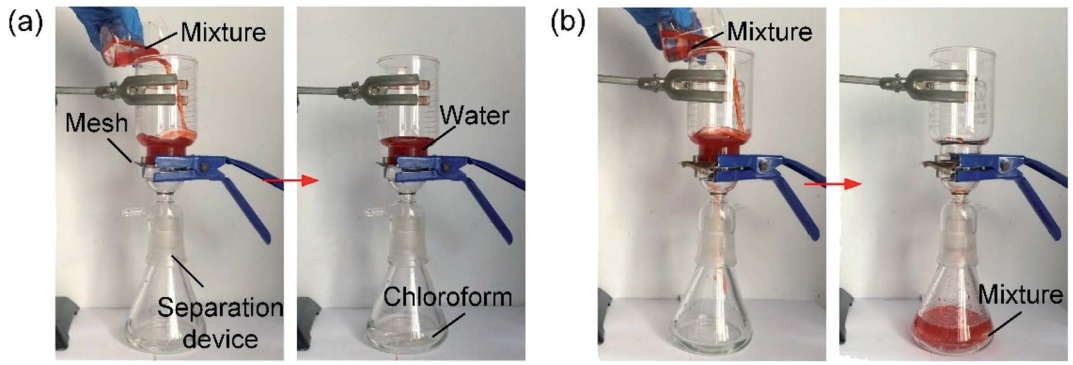

Fig. 9 Separation of the mixture of water and chloroform using the abraded mesh based on the (a) underoil superhydrophobicity and (b) superhydrophobicity.

calculated by separation efficiency = liquid collection (g)/liquid (g) × 100%, where the liquid was chloroform. After 10 abrasion cycles, the oil–water separation process of the abraded mesh was demonstrated based on the underoil superhydrophobicity of the mesh, and the separation efficiency was as high as 97.8%, indicating that the abraded mesh maintained an excellent oil–water separation property, as shown in Fig. 9a. Moreover, as expected, the abraded mesh could maintain high separation efficiency even after 10 successive separations based on the underoil superhydrophobicity, and the separation efficiency was above 97%, as shown in Fig. S3.† However, by using the superhydrophobicity in the chloroform–water separation process, the oil–water separation of the abraded mesh failed, as shown in Fig. 9b. Therefore, the mesh based on the prewetting induced underoil superhydrophobicity was more appropriate for the oil–water separation than that based on the superhydrophobicity.

4. Conclusions

This study presents a simple fabrication method of underoil superhydrophobic surfaces based on laser-ablated technology, which does not require any chemical modification. The proposed method is suitable for large-scale and mass production of underoil superhydrophobic materials. The sandpaper abrasion test is performed to verify the durability of the underoil superhydrophobic surfaces fabricated by the proposed fabrication method. Test results demonstrate that the fabricated surfaces have a more durable water-repellent property in oil than in air. Moreover, based on the underoil superhydrophobicity, the abraded surfaces (meshes) can maintain steady self-cleaning property and oil–water separation. This work can provide helpful guidance for the fabrication of underoil superhydrophobic surfaces, which could be useful for further research of wettability, self-cleaning and oil–water separation in practical applications.

Conflicts of interest

There are no conflicts to declare.

Acknowledgements

This work was supported by the China Postdoctoral Science Foundation (No. 2019M661184), the 13th Five-Year Scientific and Technological Research Project of the Education Department of Jilin Province (No. JJKH20200746KJ), the Science and Technology Innovation Fund of CUST (No. XJJLG-2019-05), and the "111" Project of China (No. D17017).

References

1 M. J. Liu, S. T. Wang and L. Jiang, Nature-inspired superwettability systems, *Nat. Rev. Mater.*, 2017, **2**(7), 17036.
2 T. Darmanin and F. Guittard, Superhydrophobic and superoleophobic properties in nature, *Mater. Today*, 2015, **18**(5), 273–285.
3 Z. X. Lian, J. K. Xu, Z. B. Wang, *et al.* Biomimetic superlyophobic metallic surfaces: focusing on their fabrication and applications, *J. Bionic Eng.*, 2020, **17**(1), 1–33.
4 M. J. Kreder, J. Alvarenga, P. Kim, *et al.* Design of anti-icing surfaces: smooth, textured, or slippery?, *Nat. Rev. Mater.*, 2016, **1**(1), 15003.
5 B. Wang, W. X. Liang, Z. G. Guo, *et al.* Biomimetic superlyophobic and super-lyophilic materials applied for oil/water separation: a new strategy beyond nature, *Chem. Soc. Rev.*, 2014, **44**(1), 336–361.
6 X. T. Han and X. Gong, *In situ*, one-pot method to prepare robust superamphiphobic cotton fabrics for high buoyancy and good antifouling, *ACS Appl. Mater. Interfaces*, 2021, **13**, 31298–31309.
7 J. K. Xu, Q. Q. Cai, Z. X. Lian, *et al.* Research progress on corrosion resistance of magnesium alloys with bio-inspired water-repellent properties: a review, *J. Bionic Eng.*, 2021, **18**, 735–763.
8 S. Rasouli, N. Rezaei, H. Hamedi, *et al.* Design, fabrication, and characterization of a facile superhydrophobic and superoleophilic mesh-based membrane for selective oil–water separation, *Chem. Eng. Sci.*, 2021, **236**, 116354.
9 J. Zhang, L. Zhang and X. Gong, Large-scale spraying fabrication of robust fluorine-free superhydrophobic coatings based on dual-sized silica particles for effective

antipollution and strong buoyancy, *Langmuir*, 2021, **37**(19), 6042–6051.

10 C. Chen, D. Weng, S. Chen, *et al.* Development of durable, fluorine-free, and transparent superhydrophobic surfaces for oil/water separation, *ACS Omega*, 2019, **4**(4), 6947–6954.

11 Z. X. Lian, J. K. Xu, Z. J. Yu, *et al.* Bioinspired reversible switch between underwater superoleophobicity/superaerophobicity and oleophilicity/aerophilicity and improved antireflective property on the nanosecond laser-ablated superhydrophobic titanium surfaces, *ACS Appl. Mater. Interfaces*, 2020, **12**(5), 6573–6580.

12 T. Verho, C. Bower, P. Andrew, *et al.* Mechanically durable superhydrophobic surfaces, *Adv. Mater.*, 2011, **23**(5), 673–678.

13 X. L. Tian, T. Verho and R. H. A. Ras, Moving superhydrophobic surfaces toward real-world applications, *Science*, 2016, **352**(6282), 142–143.

14 P. C. Zhang, S. S. Wang, S. T. Wang, *et al.* Superwetting surfaces under different media: effects of surface topography on wettability, *Small*, 2015, **11**(16), 1939–1946.

15 M. M. Liu, J. Li and Z. G. Guo, Electrochemical route to prepare polyaniline-coated meshes with controllable pore size for switchable emulsion separation, *Chem. Eng. J.*, 2016, **304**, 115–120.

16 X. L. Tian, V. Jokinen, J. Li, *et al.* Unusual dual superlyophobic surfaces in oil–water systems: the design principles, *Adv. Mater.*, 2016, **28**(48), 10652–10658.

17 Y. Lu, S. Sathasivam, J. L. Song, *et al.* Robust self-cleaning surfaces that function when exposed to either air or oil, *Science*, 2015, **347**(6226), 1132–1135.

18 C. L. Xu and Y. Z. Wang, Durability, anti-corrosion and self-clean in air/oil of a transparent superhydrophobic polyimide film, *Appl. Mater. Today*, 2018, **10**, 18–23.

19 G. L. Cao, W. B. Zhang, Z. Jia, *et al.* Dually prewetted underwater superoleophobic and under oil superhydrophobic fabric for successive separation of light oil/water/heavy oil three-phase mixtures, *ACS Appl. Mater. Interfaces*, 2017, **9**(41), 36368–36376.

20 H. Y. Lai, A. D. Leon, K. Pangilinan, *et al.* Superoleophilic and under-oil superhydrophobic organogel coatings for oil and water separation, *Prog. Org. Coat.*, 2018, **115**, 122–129.

21 Z. X. Lian, J. K. Xu, Z. B. Wang, *et al.* Nanosecond laser induced underwater superoleophobic and underoil superhydrophobic mesh for oil/water separation, *Langmuir*, 2018, **34**(9), 2981–2988.

22 D. V. Ta, A. Dunn, T. J. Wasley, *et al.* Nanosecond laser textured superhydrophobic metallic surfaces and their chemical sensing applications, *Appl. Surf. Sci.*, 2015, **357**, 248–254.

23 J. Zimmermann, F. A. Reifler, G. Fortunato, *et al.* A simple, one-step approach to durable and robust superhydrophobic textiles, *Adv. Funct. Mater.*, 2008, **18**, 3662–3669.

24 K. L. Chen, S. X. Zhou, S. Yang, *et al.* Fabrication of all-water-based self-repairing superhydrophobic coatings based on UV-responsive microcapsules, *Adv. Funct. Mater.*, 2015, **25**, 1035–1041.

25 Y. Hou, Z. Wan, J. Guo, *et al.* Facile fabrication of robust superhydrophobic porous materials and their application in oil/water separation, *J. Mater. Chem. A*, 2015, **3**, 23252–23260.

26 L. T. Yin, J. Yang, Y. C. Tang, *et al.* Mechanical durability of superhydrophobic and oleophobic copper meshes, *Appl. Surf. Sci.*, 2014, **316**, 259–263.

27 K. L. Chen, Y. Wu, S. X. Zhou, *et al.* Recent development of durable and self-healing surfaces with special wettability, *Macromol. Rapid Commun.*, 2016, **37**(6), 463–485.

28 X. S. Jing and Z. G. Guo, Biomimetic super durable and stable surfaces with superhydrophobicity, *J. Mater. Chem. A*, 2018, **6**(35), 16731–16768.

29 R. N. Wenzel, Resistance of solid surfaces to wetting by water, *Ind. Eng. Chem.*, 1936, **28**, 988–994.